AIAA 2003-3113

Computational Study of Porous Treatment for Altering Flap Side-Edge Flowfield

Meelan Choudhari and Mehdi R. Khorrami
NASA Langley Research Center
Hampton, Virginia

9th AIAA/CEAS Aeroacoustics Conference
May 12–14, 2003
Hilton Head, South Carolina

AIAA-2003-3113

Computational Study of Porous Treatment for Altering Flap Side-Edge Flow Field*

Meelan Choudhari[1] and Mehdi R. Khorrami[2]
NASA Langley Research Center
Hampton, Virginia

Abstract

Reynolds-averaged Navier-Stokes calculations are used to investigate porous side-edge treatment as a passive means for flap noise reduction. Steady-state simulations are used to infer effects of the treatment on acoustically relevant features of the mean flow near the flap side edge. Application of the porous treatment over a miniscule fraction of the wetted flap area (scaling with the flap thickness) results in significantly weaker side-edge vortex structures via modification of the vortex initiation and roll-up processes. At high flap deflections, the region of axial flow reversal associated with the breakdown of the side-edge vortex is also eliminated, indicating an absence of vortex bursting in the presence of the treatment. Potential ramifications of the mean-flow modifications for flap-noise reduction are examined in the light of lessons learned from recent studies on flap noise. Computations confirm that any noise reduction benefit via the porous treatment would be achieved without compromising the aerodynamic effectiveness of the flap. Results of the parameter study contribute additional insight into the measured data from the 7x10 wind tunnel at NASA Ames and provide preliminary guidance for specifying optimal treatment characteristics in terms of treatment location, spatial extent, and flow resistance of the porous skin.

1. Introduction

Noise radiation from flap side edges is known to be a major component of non-propulsive, i.e., airframe-generated noise.[1,3,8,9,17,23] Due to continued success in reducing the engine noise levels, the non-propulsive sources of noise have emerged as a bottleneck to further reductions in aircraft acoustic emissions, especially during the aircraft approach for landing. Recent investigations of airframe noise[2,13,20,21,23] have focused on developing physics-based noise reduction techniques, i.e., on concepts that are derived from an established cause-effect relationship between sources of near-field unsteadiness and far-field noise. This paper targets one specific application of this investigative paradigm: the application of a permeable (porous) skin segment along the flap-tip surface to alter the local flow features suspected as the primary cause behind noise generation near the side edge.

The noise producing features near a flap side edge include[10,11,25,26]: free shear layers and their rollup, formation of multiple vortices, vortex merging, and even vortex bursting when the flap deflection is sufficiently large. Because of the significant unsteadiness sustained by the above features and their close proximity to the corners along the edge surface, these features are likely to contribute a substantial portion of the overall noise radiation from the flap side edge[10,25,26]. Consequently, any flow control strategy that targets (i) the vortex initiation regime, (ii) the intensity of the vortex roll-up, and/or (iii) the vortex breakdown near the flap trailing edge without an adverse impact on the remaining processes is likely to produce a significant noise reduction benefit. Several such strategies have been investigated in recent experiments on flap-edge noise. The list includes both passive devices (such as a side-edge fence[21,23], a rounded[23] and/or yawed side edge[23], a porous tip treatment[2,20,23], flap-tip brush[2], and continuous moldline technology[24]) and active blowing through the flap side edge[13]. Despite their common themes, these devices are known to differ significantly in the details of the physical mechanisms underlying the noise reduction, the resulting reduction in far-field noise, and their suitability for deployment on a flight platform. In the

[1]Aerospace Technologist, Computational Modeling and Simulation Branch, Senior Member AIAA
[2] Aerospace Technologist, Computational Modeling and Simulation Branch, Associate Fellow AIAA

latter regard, passive devices are particularly attractive because of their simplicity and the limited duration over which the high-lift systems are operative.

The side-edge fence delays the roll-up of the shear layer and locks the position of the side-edge vortex near the bottom edge, so it cannot merge with the vortex along the top edge and form a single dominant vortex. Measurements by Storms et al.[23] on a two-element, unswept high-lift configuration suggested that the noise reduction benefit from a side edge fence may be limited to 3dB (or less, depending on the tip rake angle). However, other experiments[3,21] have yielded higher reductions, up to 7 dB in the case of ref. [21]. The side-edge fence is expected to add a small amount of weight to the high-lift system, which must be carried during the entire flight. A non-retractable fence could also be accompanied by a drag penalty during the cruise segment.

In contrast, a porous flap-tip treatment was found to reduce the flap side edge noise by 4-8 dB across a wide range of frequencies,[23] without incurring a loss of lift. A treatment of this type is simple to implement, and has advantages in terms of weight, cost and maintenance. As indicated by Frink et al.,[5] it is also possible to design an adaptive porous surface that can be actuated at will. Thus, the porous tip treatment should be easy to integrate on both new and existing commercial aircraft. The dual mechanism conjectured for the effectiveness of the porous tip treatment involves, first, a modification of local mean-flow structures due to flow leakage across the permeable skin and, second, the damping effect of a finite impedance surface on the pressure fluctuations in the near-field. The role of active blowing through localized apertures is somewhat analogous to the first of these mechanisms; however, the second mechanism would be absent in the case of blowing. To what extent this difference will account for the reduced noise benefit from the active strategy[13] (versus the passive porous tip[2,20,23]) remains to be seen.

The recently proposed concept of continuous moldline technology (CMT) would eliminate exposed flap side edges by smoothly connecting the flap edge with the adjacent wing surface[24]. This technique should effectively suppress the noise sources associated with flap noise. Of course, careful aerodynamic design is necessary to avoid adverse aerodynamic impact due to the modified flap design. The CMT concept may not be suitable for retrofitting onto high-lift systems designed for Fowler flaps, or in cases where no adjacent surface exists, such as wing tips or fan rotor tips[12]. Thus, a porous tip treatment should be a viable alternative to CMT in these cases.

Besides establishing the noise reduction benefit from the porous-tip treatment, measurements made during the collaborative experiments of Lockheed-NASA Ames-Boeing[20,23] provided valuable clues to the underlying physics of noise generation. The goal of this paper is to report on complementary, Reynolds averaged Navier-Stokes (RANS) calculations of the side-edge flow field. By readily providing details of the mean flow near the side edge, numerical simulations of this type can provide additional insights for further development of the porous tip treatment. To that end, the following questions are addressed in this study:

1. investigate both the modifications to noise-producing mean-flow structures as a result of the porous-edge treatment and the potential implications of these modifications for the intensity of flap noise, and
2. demonstrate the feasibility of designing a porous edge treatment with a minimal surface area and, hence, minimum aerodynamic penalty.

To meet these objectives, the effects of the treatment are examined in light of the lessons learned from recent airframe noise investigations.

An outline of the paper is as follows. A brief description of the computational modeling of the porous tip is given in section 2. Section 3 provides an overview of the changes in the flap side-edge flow for one particular set of treatment design parameters. In section 4, we present the results from a limited parametric study within the design space and use them to infer optimal characteristics of the porous-tip treatment. Conclusions are presented in section 5.

2. Computational Approach

2.1 Modeling of Porous Flap Tip

The porous tip configuration envisioned here is conceptually similar to that used during the experiments in the 7x10 wind tunnel at NASA Ames[22,23]. Specifically, a permeable (or porous) skin is applied along small but appropriately selected portions of the flap surface near the side edge. The hollow tip volume (or plenum) underneath the porous segments permits passive leakage of flow from the high-pressure region of the tip surface (typically along the flap bottom) to the low-pressure regions (along the side edge and the top surface); the leakage flow, in turn, allows a modified vortex structure to be established near the flap side edge. In computing the alterations to such macroscopic features of the side-edge flow, it is neither desirable nor necessary to include the details of the flow in the immediate vicinity of the pores on the treated surface.

We assume that both the length scales associated with the porous-skin configuration and the resulting leakage-flow velocities are suitably small. In that case, effects of the porous treatment on the side-edge flow can be captured by the combination of a local jump condition between the area-averaged flow quantities on each side of the treatment surface and a model for the flow within the plenum chamber underneath. Both of the above criteria can be met by using treatment surfaces fabricated from a finely woven porous skin. The constraint on the maximum leakage velocities further implies that the plenum pressure may be treated as nearly uniform, which allows the dynamics of the plenum flow to be excluded from the calculations.

The above considerations lead to the following jump condition between the area averaged transpiration velocity V_n, pressure p and density ρ at the exterior of the porous skin, and the plenum pressure p_p:

$$V_n = \beta\,(p_p - p) / M \qquad (1)$$

where $\beta = \beta^* \rho^* U^*$ is the steady (dc) flow admittance (i.e., inverse of dc flow resistance) scaled with respect to the momentum of the free-stream flow. All other non-dimensional quantities are scaled by using the free-stream density and speed of sound. The hydrodynamic (rather than acoustic) scaling for the surface admittance parameter β reflects the primarily hydrodynamic role of the porous treatment. The plenum pressure p_p is determined via the constraint of passive porosity, which requires the net mass flux across the permeable segments to be zero. Remaining boundary conditions at the porous skin (i.e., those for the tangential velocity components and the wall temperature) are assumed to remain the same as the untreated solid surface.

In general, the dc flow admittance is an algebraic function of the surface-normal velocity V_n. For viscosity dominated flow across the porous skin, β may be assumed to be constant, i.e., $\beta = \beta_0$ (where β_0 is independent of V_n). In such cases, the jump condition across the porous skin reduces (in the low-speed limit) to a strictly linear relation between velocity and pressure. The linear relationship has been used in a number of earlier studies related to the aerodynamic effects of passive porosity[5,19], particularly in the context of wave drag reduction. In reality, of course, the inertial (nonlinear) effects cannot be discounted when the transpiration velocities becomes sufficiently large. At this stage, the surface pressure differential $p-p_p$ driving the leakage flow is more appropriately treated as a quadratic function of V_n (i.e., $\beta \rightarrow \beta_0/(1+N|V_n|/M)$, where N is the nonlinear coefficient). Finely woven porous skins correspond to smaller values of N in comparison with larger sized perforates. The perforates become nonlinear at smaller leakage velocities, resulting in a larger uncertainty in the distribution of the in-situ flow admittance (and, hence, in the effectiveness of the porous treatment).[20]

Earlier studies have proposed more refined nonlinear models that account for the dependence of pressure loss across the skin on both magnitude and direction of the local transpiration velocity[6]. The higher fidelity, however, requires specifying additional details of the porous surface. In the interest of generality, and to keep the model sufficiently simple at this stage, the linear model was adopted for the present calculations. A limited assessment of the nonlinear effects is presented in section 3.2 below.

Note that the porous skin treatment modeled herein is somewhat different from the bulk porosity used by Chow et al.[2], which appeared to provide a more modest noise reduction benefit (<2dB) compared with the porous skin.

2.2 Description of Flow Configuration and Modified RANS Solver

The model for the porous surface treatment outlined in Section 2.1 was incorporated into the CFL3D[14] code developed at NASA Langley Research Center, and was used to assess the effects of the porous treatment on the flap-edge flow field within the two-element high-lift configuration used in the 7x10 experiments at NASA Ames[23]. This choice of flow configuration was motivated by the fact that the baseline case (i.e., untreated flap) for this geometry has been extensively scrutinized in recent work involving experiments in the 7x10 tunnel at NASA Ames[22,23] and the open jet Quiet Flow Facility (QFF) facility at NASA Langley,[17] and steady RANS computations[10,15]. The satisfactory agreement between the computed flow field and measured data for both on- and off-surface quantities near the flap side edge made the 7x10 configuration an ideal setting for further computations involving a noise reduction device. As mentioned previously, additional measurements in the 7x10 tunnel included aerodynamic and noise data in the presence of the porous flap treatment.

The un-swept model geometry used in the 7x10 experiments includes a NACA 63_2-215 Mod B wing and a half-span, slotted flap with 30 percent chord length (Fig. 1). The flap tip is flat, with sharp edges along the intersections with the top and bottom surfaces of the flap. The model chord in the stowed position is 2.5 ft, i.e., approximately 15 percent of the values for a typical

medium sized commercial transport. Throughout the computations reported in this paper, the main element angle of attack was held fixed at 10 degrees, while two flap deflections (29 and 39 degrees, respectively) were examined. The free-stream Mach number was set to 0.2 (versus 0.22 in the 7x10 experiments) and the Reynolds number based on the clean airfoil chord was equal to 3.7 million , identical to that in the 7x10 experiments.

The structured multi-block grid was the same as that used during the earlier calculations for the untreated case[10]. This grid was designed to provide an adequate resolution of the dominant mean-flow structures near the flap side edge and contained approximately 4.5 million points distributed over 16 blocks. For further details about the model geometry, computational grid, flow solver and choice of algorithmic parameters used for the simulations, the reader is referred to Ref. [10]. Ref. 10 also addresses the grid independence of the baseline solution, demonstrating good agreement with the measured surface pressures and off-surface vortex structures. Accordingly, the finest grid from Ref. [10] was chosen for the present study, and no additional grid convergence studies were considered necessary for assessing the changes in the computed flow field due to the flap side-edge treatment. CFL3D implementations of Spalart-Allmaras and Menter's shear stress transport (SST) models were used to establish that the inferred flow-field modifications were not specific to any given turbulence model.

Table 1 provides an outline of the various tip treatment options examined herein. In all cases, the maximum spanwise extent of the treated region is limited to approximately 4 percent of the flap span, i.e., about 1.35 times the maximum flap thickness. To reduce the computational cost associated with these cases, the converged solution for the baseline case was used as the initial condition for each set of treatment parameters from Table 1. Furthermore, to accelerate the overall convergence without triggering significant unsteadiness (in spite of the highly resolved flap-edge grid), the admittance parameter was gradually ramped up to its final value over a fixed number of iterations. The plenum pressure was lagged behind the other flow variables and the value of p_p was updated at each iteration in order to drive the net mass flux across the porous surface to zero. Typically, this procedure was adequate, as indicated by the convergence history in Fig. 2 for both the plenum pressure p_p and the net mass flux (scaled by the mass flux across the bottom section of the porous skin). Although all of the computed solutions have not yet been thoroughly reviewed, the analysis completed thus far permits a preliminary assessment of the various treatment options as described in sections 3 and 4 below.

Table 1: Treatment Configurations Examined During the Study

(Δz and Δx denote the spanwise and chordwise extents of the treated region, respectively; the normalizing length scales b and c_f refer to the flap span and chord, respectively.)

Case	Treatment Configuration	β_0
A04	Aft section only; linear	0.04
A10	$\Delta z/b \approx 4\%$	0.10
A16	$\Delta x/c_f \approx$ Aft 78%	0.16
A32		0.32
LE10	Leading edge included	0.10
LE16	(i.e., full chord) $\Delta z/b \approx 4\%$ $\Delta x/c_f \approx 100\%$	0.16
BS16	A16 with bottom segment sealed	0.16
TS16	A16 with top segment sealed	0.16
SS16	A16 with side edge sealed	0.16
A10NL	A10 with velocity dependent flow admittance (N=10)	0.10
A16NL	A16 with velocity dependent flow admittance (N=10)	0.16

3. Mean-Flow Modifications Due to a Porous Flap Tip

A majority of the computations were carried out for a flap deflection of 29 degrees, the angle at which the side-edge noise first became dominant during the microphone array measurements by Storms et al[23]. We begin with a comparison of the baseline solution for this configuration with the flow field modified by using treatment option A16 from Table 1 (i.e., linear, aft-only treatment with β_0=0.16).

3.1 Structural Changes in Side-Edge flow

Figs. 3a and 3b illustrate the overall effects of the porous edge configuration A16 on the vortex structures near the flap side edge as visualized through corresponding distributions of streamwise vorticity at selected locations along the flap chord. The baseline solution (Fig. 3a) clearly depicts the formation of a dual vortex system as established in prior measurements[23,24] and computations.[10] Flow separation along the bottom edge of the tip surface leads to the formation of a shear layer, which quickly rolls up into a strong vortex adjacent to the tip surface. A weaker vortex of similar

circulation is formed along on the top surface, due to secondary separation along the top edge. Due to the smaller inclination of the side-edge vortex compared with the flap deflection angle, the location of the side vortex shifts upward relative to the tip contour at farther downstream locations. As a result, the side-edge vortex crosses over to the top surface near the flap mid-chord location, quickly engulfing the weaker top-edge vortex. The merged vortex continues to gain strength over the downstream section of the flap, with the help of additional vorticity fed by the shear layer from the bottom edge. The increased spatial scales of the mean-flow structures correlate well with the measured dominance of low-frequency noise sources in the downstream direction.

For the treated case (Fig. 3b), lack of surface treatment near the flap leading edge results in vortex initiation and formation patterns that are nearly identical to the baseline case. However, streamwise vorticity contours over the treated portion of the flap display a significant alteration of the local flow field. In the mid-chord region of the flap, the porous treatment incites a weakening of the main side-edge vortex. An equally beneficial effect of transpiration through the porous segments is an elbowing of the side and top vortices and the connecting shear layers away from the edge solid surfaces (x = 1.04 in Fig. 3b). In contrast to the baseline flow field, interaction between the two vortices aft of the mid-chord region is a slow and benign process that takes place far above the flap surface and never culminates into in a fully merged single vortex. This slow dance between the two vortices is caused by a substantial weakening of the main vortex that no longer can dominate or accelerate the merging process. Towards the flap trailing edge, the established flow can be described as a diffuse vortical flow structure that spreads over a larger spatial extent than the corresponding baseline field. As shown in section 3.3 below, the total lift and hence the amount of vorticity in the side vortex remains unaffected by the porous treatment; however, the porosity induced leakage simply redistributes this vorticity over a significantly larger region.

In both of the solutions shown in Figs. 3a and 3b, locations of the dominant edge vortices correlate well with the pressure isosurfaces associated with lower pressures within the vortex cores. Because vorticity distribution is frame-dependent, we choose henceforth to assess the effects of the porous treatment using changes in the static pressure distributions. In Figs. 4-7, the comparison of side-edge flow structures has been reinterpreted via a closer scrutiny of the corresponding Cp distributions across a series of chordwise cross sections. It is important to note that the contour range for the treated case has been suitably adjusted to maintain a similar visual appearance, so that the distinction between the vortex structures in the treated and untreated solution should be inferred by using the respective range of contour values.

Immediately after the beginning of the treatment (at $x/c_f \approx 22\%$), the low-pressure footprint of the vortex adjacent to the bottom edge leads to an outward mass flux through the side edge, which in turn pushes the vortex and the shear layer that feeds vorticity to the vortex slightly further away from the edge surface (Fig. 4). As discussed previously, the side-edge vortex in the treated case is already somewhat weaker, and its movement upward is significantly faster than the baseline case. Both of these trends continue through the mid-chord region, so that the weakened side-edge vortex in the treated case has already been pushed over the top edge at x = 1.04 (i.e., $x/c_f \approx 43.7\%$). An important flow feature at x=1.06 modified by the porous treatment is the region of intense flow acceleration (lowest pressures) that occurs near the top corner along the mid-chord region. These extreme pressure lows correspond to the foot print of the side vortex scrubbing against the edge within this region. In other words, downwash due to the vortex accelerates the spanwise flow along the top surface past the sharp corner, resulting in a small pocket of opposite sign vorticity that eventually evolves into a vortex. The surface treatment essentially replaces the pressure minimum with a milder variation in surface pressures along the edge. In doing so, the treatment has probably weakened a potential hot spot where high frequency, high amplitude pressure fluctuations would have been generated.

Additional spanwise flow around the bottom edge creates a secondary side edge vortex along the aft portion of the flap chord; however, this vortex is also relatively weak. It appeared to gain some strength along the chord; however, its lateral location is still farther away from the tip surface, indicating a weaker footprint along the side edge.

The vertical position of the core of the merged vortex in the treated case continues to be further removed from the top surface (compared to the baseline case) up to about x=1.11 ($x/c_f \approx 73\%$), after which it does not seem to be significantly influenced by the weak blowing from the relatively distant top surface. However, the strong disparity between the contour values throughout the downstream sections reaffirms the substantially weaker strength of the side-edge vortex in the presence of the

treatment. The reduced effect of porosity on the location of the post-merger vortex may be unique to the 7x10 geometry, because the vortex moves up more rapidly in this case compared with other models more closely related to commercial aircraft.

We also note that the computed effect of the distributed leakage flow in the form of weaker, more diffuse vortex structures in the vicinity of the side edge is qualitatively analogous to that of localized blowing within the side edge region as observed from PIV measurements[13].

3.2 Acoustic Implications of Mean-Flow Modifications

Without any modeling of the near-field unsteadiness, it is not possible to translate the above flow alterations into accompanying reduction in the sound pressure levels. However, qualitative speculations about the physical mechanisms responsible for flap side-edge noise can be made based on microphone array measurements of side-edge noise, findings related to ad hoc noise reduction devices, and recently proposed theoretical models. Information from these sources strongly suggests that a dominant fraction of the far-field noise should be attributed to an interaction between the flap-tip surface and the large-scale unsteady disturbances riding on and amplified by the dominant mean-flow structures that were discussed in section 3.1.

Foremost among the prominent unsteady fluctuations are the natural modes of oscillation of the free shear layers and vortices that appear along the side edge. These mostly inviscid disturbances are amplified over a convective length scale and, thus, can achieve high amplitudes rather rapidly. Their rate of growth depends directly on the magnitude of the shear (i.e., vorticity) in the background mean velocity field. To lessen the magnitude of the unsteadiness projected onto the flap edge surfaces, a noise reduction strategy must either diffuse the local vorticity field prematurely or push the source of hydrodynamic fluctuations away from the edge surfaces. As elucidated in the previous paragraphs, both of these tasks are achieved rather effectively with the application of porous treatment. A rather important added benefit of the porous treatment is the suction of the turbulent boundary layer near the edge on the flap bottom surface. In a traditional point of view, the passage of the boundary layer over the edge is cause for conversion of turbulent fluctuations into pressure fluctuations and thus broadband acoustic scattering from the sharp edge. By effectively removing this turbulent layer, it is anticipated that acoustic radiation from the bottom edge for the treated case would be substantially reduced.

The only additional information about near-field unsteadiness that can be readily derived from a steady RANS computation corresponds to the turbulence kinetic energy (TKE) field predicted by the two-equation SST model. Unlike laboratory measurements of simpler vortex flows, which indicate that peak fluctuation levels occur outside of a nearly laminar vortex core, most linear eddy viscosity models predict peak levels of TKE at the center of the vortex. Despite this deficiency, it seems plausible to infer aeroacoustic trends related to the porous treatment from resulting changes in the predicted TKE levels. Similar ideas have been commonly applied to other sources of aircraft noise; however, given the lack of relevant physics in the turbulence model concerning the large-scale structures responsible for airframe noise, such interpretations in the context of airframe noise must be treated with caution.

A comparison of the TKE distributions predicted by the turbulence model for the baseline and treated case (configuration A16 in Table 1) is shown in Figs. 8a-b. Once again, the reader is reminded of the scale disparity between the two plots. The treatment reduces the peak TKE levels associated with the merged vortex near the trailing edge by a factor of 2.5; comparable reductions are observed for the vortex adjacent to side edge near the mid-chord region. The predictions based on TKE distribution are, therefore, qualitatively consistent with the earlier observations based on the paradigm of hydrodynamic stability (i.e., large-scale, unsteady structures).

3.3 Aerodynamic Metrics and Low-Order Measure for Treatment Effectiveness

Consistent with the measured data in the 7x10 wind tunnel, the computed lift coefficients for the untreated and treated cases indicate negligible changes due to the porous treatment. The momentum flux associated with the leakage flow had a negligible influence on the overall lift. Thus, impact of the noise reduction device on aerodynamic efficiency of the flap should not be a factor during integration of the porous tip concept on a flight platform. Sectional lift distribution over the flap (Fig 9) shows that the loss of vortex lift due to the leakage flow is compensated by increased lift coefficients farther inboard, presumably because of the reduced downwash (and, perhaps, a slightly lower induced drag) associated with the weaker flap-tip

vortex. The extended influence of the porous treatment in spite of its localized application is consistent with the expectations on the basis of the lifting line theory[20].

The increasingly smooth spanwise variation in the sectional lift coefficient at higher values of β_0 is to be expected, as the accompanying increase in flow leakage tends to reduce the pressure differential across the top and bottom surfaces (flap loading) in the vicinity of the side edge. Because the associated changes in the off-surface flow structures are reasonably correlated with this behavior, in section 4, we will use the chordwise Cp distribution adjacent to the side edge as an approximate, low-order measure to assess the relative effectiveness of alternative treatment configurations.

4. Effects of Flap Deflection Angle and Treatment Design/Modeling Parameters

4.1 Flap Deflection of 39 Degrees

Computations for the flap deflection of 39 degrees revealed changes in side-edge flow similar to those discussed in section 3 for a flap deflection of 29 degrees. Because of the higher flap loading at 39 degrees, even a modest flow admittance of β_0=0.10 was found to be quite effective in weakening the post-merger side edge vortex. A previous study by Khorrami et al.[10] has established that the baseline solution for a flap deflection of 39 degrees exhibits an additional, somewhat curious feature that was absent at a flap deflection of 29 degrees. In particular, a rapid deceleration of streamwise velocities within the vortex core leads to a flow reversal, analogous to the vortex bursting (or breakdown) phenomenon observed in simpler flows within a pipe. Khorrami et al. speculate that bursting itself is likely to be a low-frequency phenomenon; however, it could support high-frequency fluctuations in the immediate vicinity of the side-edge surface and, hence, contribute significantly to the far-field noise. Although not shown, the present calculations indicate the effectiveness of the porous treatment in preventing the breakdown of the side-edge vortex, which might account for another aspect of its noise reduction capability.

4.2 Surface Permeability

By controlling the magnitude of the leakage flow, the flow admittance parameter can exert a critical influence on the flap-edge vortex structures and, hence, on the aeroacoustic effectiveness of the porous tip treatment. Recall that, due to the primarily hydrodynamic role of the treatment in influencing the side-edge flow field, the relevant non-dimensional parameter is $\beta = \beta^*\rho^*U^*$, rather than the specific acoustic admittance $\beta^*\rho^*c^*$. To quantify the potential sensitivity of the mean-flow alterations to the flow admittance parameter, we examined the changes in static Cp distributions near the side edge as β_0 is increased from 0.0 (untreated case) to 0.32 for the aft-only treatment configuration in Table 1. Figure 10 shows that these changes clearly quantify the progressive weakening of the vortex structures resulting from a corresponding reduction in the magnitude of the suction peak near the mid-chord location. The reduction in the suction peak from β_0=0.16 to β_0=0.32 is rather marginal, suggesting that a point of diminishing returns may have been reached in terms of further weakening of the vortex structures. For the A16 treatment configuration, the average leakage velocity across the treated section of the side edge is approximately equal to 6 percent of the free-stream speed, with the peak velocities approaching 8 percent to 10 percent.

Furthermore, the peak TKE levels decreased with each increase in β_0 up to 0.32, indicating a corresponding decrease in the strength of noise sources. However, we note that the increased values of β_0 also lead to a stronger discontinuity in surface impedance at the boundary between the treated and untreated portions of the flap surface. The increased scattering of near-field fluctuations near this discontinuity might partially offset the monotonic benefit due to reduced amplitude fluctuations at larger values of β_0.

4.3 Spatial Extent

Storms et al[23] measured the acoustic effects of sealing off selected portions of the porous treatment surface used in their experiments. The porous treatment was found to be effective when applied only within a narrow vicinity of the side edge. This conclusion was anticipated a priori in the present study, based on theoretical considerations related to the size of footprint of the side-edge vortex along the flap suction surface. Somewhat analogous to the investigation of Ref. [23], we studied the consequences of selectively sealing off the bottom, side, and top segments of the treatment surface. The resulting Cp distributions along the top edge are roughly analogous for all three of these cases (Fig. 11). Essentially, the low-pressure footprint around the mid-chord location is weakened relative to the untreated case, but not as much as the A16 treatment configuration with all three segments open. Although neither of the above three cases is likely to be a candidate for optimal design, further scrutiny of the computed flow alterations and coordinated experiments

could provide additional insight into the physics of the noise generation process.

Extending the porous skin up to the leading edge helped reduce the strength of the top edge vortex (Fig. 12); however, porosity near the leading edge also leads to strong inflow along the stagnation region (substantially reducing the leading-edge suction peak along the top edge) and a weak outflow along the inboard section of the top surface near the leading edge (where it does not serve any useful purpose). The corresponding TKE distributions shown in Fig. 13 indicate a significant reduction in TKE levels relative to the aft-only treatment with the same admittance; this reduction persists through the mid-chord region. Because the front section of the side-edge region is known to dominate the high-frequency content of the far-field acoustics, extending the treated region closer to the leading edge might provide additional noise reduction benefits at the higher frequencies.

4.4 Nonlinear Flow Resistance Characteristics

Effects of velocity dependent dc flow admittance were also explored using the nonlinear pressure-velocity relation outlined in section 2.1. The value of the nonlinear admittance coefficient N was set to 10, such that the admittance reduces to one-half of its value in the infinitesimal flow limit when the leakage flow velocity reaches 10 percent of the free-stream speed. For the A16NL and A10NL configurations, effects of treatment surface nonlinearity were found to be moderate; they amounted to a reduction of the peak transpiration velocities, which led to a smoother distribution of leakage flow over each segment of the treatment surface. The reduction in overall mass flux (relative to the respective linear configuration) was comparable for the bottom, side, and top segments: all were in the range of 20-25 percent. Not surprisingly, therefore, the computed tip pressure distributions for the nonlinear porous-skin configurations (Fig. 14) are qualitatively similar to those for the corresponding linear case. This similarity suggests that the effects of moderate nonlinearity could be approximately quantified in terms of an effectively reduced value of the linear admittance parameter β_0.

The parameter study presented herein suggests that a significant noise reduction benefit could be gained by confining the porous treatment to a small fraction of the span near the trailing edge, determined by the footprint of the vortex along the aft portion of the flap suction surface. Accordingly, the relevant length scale for the spanwise extent of the treatment along the top and bottom surfaces corresponds to the maximum thickness flap thickness. The appropriate scale for the admittance of the porous surface corresponds to $(\rho^*U^*)^{-1}$, rather than the specific acoustic admittance. Admittance values resulting in average transpiration velocities comparable to five percent of the free-stream speed were found to be sufficiently effective in modifying the mean-flow structures near the side edge. Overall, however, a relatively robust performance is predicted with regard to variations in treatment characteristics.

5. Summary and Concluding Remarks

Previous experiments have shown the porous tip treatment to be an effective means for flap noise reduction without causing any apparent loss of aerodynamic efficiency of the flap. The present numerical study supports the experimental findings by quantifying the detailed effects of porous edge treatment on dominant features of the mean flow near the flap side edge.

Results showed that flow communication via distributed leakage across the treatment surface leads to reduced flap loading near the side edge. The reduced flap loading results in a reduced severity of shear layer roll-up adjacent to the side edge, a modified interaction between the side and top-edge vortices, and significantly weaker (more diffuse) vortex structures over the aft-chord region. The vortex structures are also slightly farther away from the side edge compared with the untreated case. Finally, the breakdown of the side edge vortex at higher flap deflections was also eliminated by the porous treatment.

Together with the previous work on flap-edge noise, which has established both direct and indirect connections between such mean-flow features and the far-field noise, the above findings provide a partial explanation for the measured noise reductions from porous edge treatment. In particular, the computed mean-flow alterations support the following conjectures: reduced potential of the diffuse vortex structures for amplifying both large- or small-scale unsteady disturbances; weaker interactions between these disturbances and the edge surface (due to increased distance of the highly disturbed flow regions from the side edges); and reduced fluctuations in the boundary-layer flow along the flap bottom surface. Of course, the steady computations presented herein cannot assess the relative importance of the above mechanisms in relation to the additional mechanism of reduced surface pressure fluctuations due to the finite impedance treatment surface.

Quantitative predictions for the noise reduction benefit are not possible at this stage. Indeed, no definitive predictive models based on the physics of noise source mechanisms are currently available even for the noise radiation from an untreated flap. Additional experiments in this area would contribute to the goal of designing a robust treatment configuration suitable for flight deployment. The parameter study presented herein provides preliminary guidance in that regard. Indeed, the present findings (originally obtained in 2001) were used in that capacity prior to a 26 percent model scale test at NASA Ames Research Center.

Studies with more refined physical modeling of the porous treatment are needed to assess the effects of the underlying simplifications in our computations. Spatially varying treatment characteristics to increase treatment effectiveness might also be worth exploring. With improved modeling, stationary RANS calculations of this type could be used at a modest incremental cost (relative to the cost of computing the baseline solution from the beginning) to investigate candidate treatment designs and/or to establish useful guidelines for the design process. On the other hand, the robustness of the treatment, as suggested by the present computations might obviate such computations after such design rules have been established and confirmed in future experiments.

Acknowledgments

It is a pleasure to acknowledge the enthusiastic support from Dr. R.T. Biedron and Dr. C.L. Rumsey during the modification of the CFL3D code for the implementation of permeable surface boundary condition. Useful technical discussions with Dr. C.L. Streett and Dr. V.N. Vatsa are also acknowledged.

References

1. Brooks, T.F., and Humphreys, W.M., "Flap-Edge Aeroacoustics Measurements and Predictions," J. Sound and Vib., Vol. 261, No. 1, pp. 31-74, Mar. 2003.
2. Chow, L.C., Mau, K., and Remy, H., "Landing Gears and High Lift Devices Airframe Noise Research," AIAA Paper 2002-2408, 2002.
3. Dobrzynski, W., Nagakura, K., Gehlhar, B., and Buschbaum, A., "Airframe Noise Studies on Wings with Deployed High-Lift Devices," AIAA Paper 98-2337, 1998.
4. Fink, M.R. and Bailey, D.A., "Airframe Noise reduction Studies and Clean-Airframe Noise Investigation," NASA Contractor Report 159311, 1980.
5. Frink, N., Bauer, S., and Hunter, C., "Simulation of Flows with Passive Porosity," Proc. ICAS Meeting, Toronto, Oct. 2002.
6. Frink, N., Bonhaus, D., Vatsa, V., Bauer, S., and Tinetti, A., "A Boundary Condition for Simulation of Flow Over Porous Surfaces," AIAA Paper 2001-2412, June 2001.
7. Hartwich, P.M., "Euler Study on Porous Transonic Airfoils With a View Toward Multipoint Design," AIAA Paper 91-3286, 1991.
8. Hayes, J.A., Horne, W.C., Soderman, P.T., and Bent, P.H., "Airframe Noise Characteristics of a 4.7% Scale DC-10 Model," AIAA Paper 97-1594, 1997.
9. Kendall, J.M., and Ahtye, W.F., "Noise Generation by a Lifting Wing/Flap Combination at Reynolds Numbers to 2.8×10^6," AIAA Paper 80-0035, Jan. 1980.
10. Khorrami, M.R., and Singer, B.A., "Stability Analysis for Noise-Source Modeling of a Part-Span Flap," AIAA Paper 98-2225, June 1998.
11. Khorrami, M.R., Singer, B.A., and Radeztsky, R.H., "Reynolds-Averaged Navier-Stokes Computations of a Flap-Side-Edge Flowfield," AIAA J., vol. 37, no. 1, pp. 14-22, 1999.
12. Khorrami, M.R., Li, F., and Choudhari, M., "Novel Approach for Reducing Rotor Tip Clerance-Induced Noise in Turbofan Engines," AIAA J., vol. 40, no. 8, pp. 1518-1528, 2002.
13. Koop, L., Ehrenfried, K., and Dillmann, "Reduction of Flap Side Edge Noise by Active Flow Control," AIAA Paper 2002-2469, 2002.
14. Krist, S.L., Biedron, R.T., and Rumsey, C.L., "CFL3D User's Manual (Version 5.0)," NASA/TM-1998-208444, June 1998.
15. Mathias, D.L, Roth, K.R., Ross, J.C., Rogers, S.E., and Cummings, R.M., "Navier-Stokes Analysis of the Flow About a Flap Edge," AIAA Paper 95-0185, 1995.
16. McInerny, S.A., Meecham, W.C., and Soderman, P.T., "Pressure Fluctuations in the Tip Region of a Blunt-Tipped Airfoil," AIAA J., vol. 28, no. 1, pp. 6-13, 1990.
17. Meadows, K.R., Brooks, T.F., Humphrey, W.M., Hunter, W.H., and Gerhold, C.H., "Aeroacoustic Measurements of a Wing-Flap Configuration," AIAA Paper 97-1595, 1997.
18. Melling, T.H., "The Acoustic Impedance of Perforates at Medium and High Sound Pressure Levels," J. Sound and Vib., vol. 29, no. 1, pp. 1-65, 1973.
19. Mineck, R.E. and Hartwich, P.M., "Effect of Full-Chord Porosity on Aerodynamic Characteristics of

the NACA 0012 Airfoil," NASA TP 3591, April 1996.
20. Revell, J.D., Kuntz, H.L, Balena, F.J., Horne, C., Storms, B.L., and Dougherty, R.P., "Trailing Edge Flap Noise Reduction by Porous Acoustic Treatment," AIAA Paper 97-1646, 1997.
21. Slooff, J.W., de Wolf, W.B., van der Wal, H.M.M., and Maseland, J.E.J., "Aerodynamic and Aero-acoustic Effects of Flap Tip Fences," AIAA Paper 2002-0848, 2002.
22. Storms, B.L., Takahashi, T.T., and Ross, J.C., "Aerodynamic Influence of a Finite-Span Flap on a Simple Wing," SAE Paper 951977, CA, Sept. 1995.
23. Storms, B.L., Ross, J.C., Horne, W.C., Hayes, J.A., Dougherty, R.P., Underbrink, J.R., Scharpf, D.F., and Moriarty, P.J., "An Aeroacoustic Study of an Unswept Wing With a Three-Dimensional High-Lift System," NASA/TM-1998-112222, Feb. 1998.
24. Storms, B.L., Hayes, J.A., Jaeger, S.M., and Soderman, P.T., "Aeroacoustic Study of Flap-Tip Noise Reduction Using Continuous Moldline Technology," AIAA Paper 2000-1976, 2000.
25. Streett, C.L., Lockard, D.P., Singer, B.A., Khorrami, M.R., and Choudhari, M.M., "In Search of the Physics: The Interplay of Experiment and Computation in Airframe Noise Research; Flap-Edge Noise," AIAA Paper 2003-0979, 2003.
26. Streett, C.L., "Numerical Simulations Leading to Noise in a Flap Side-Edge Flow Field," AIAA Paper 98-0628, 1998.

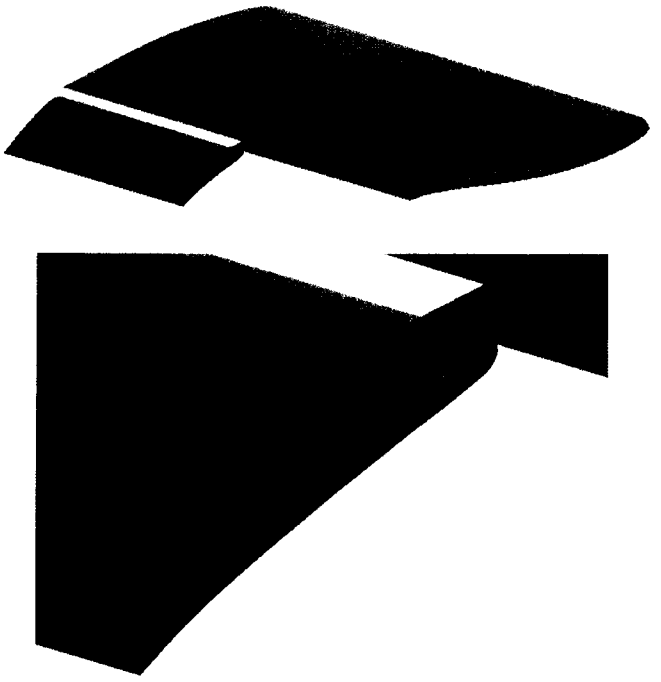

Figure 1. Model geometry and schematic of treated surfaces. The cyan region depicts the aft-only configuration in Table 1; the green mesh shows the additional area included in the LE configurations.

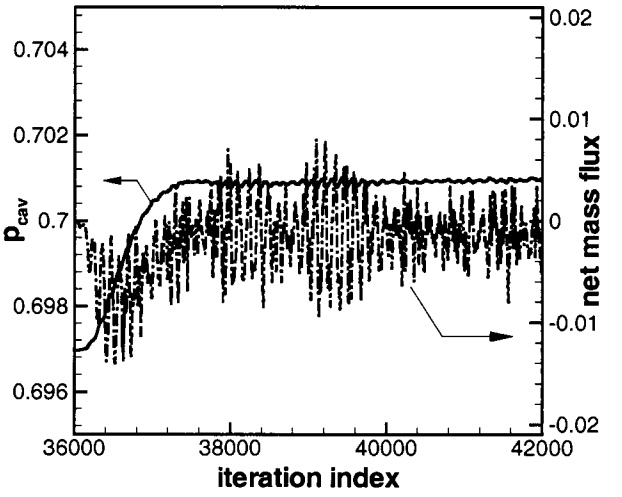

Figure 2. Convergence history of plenum pressure and net mass flux across porous segments

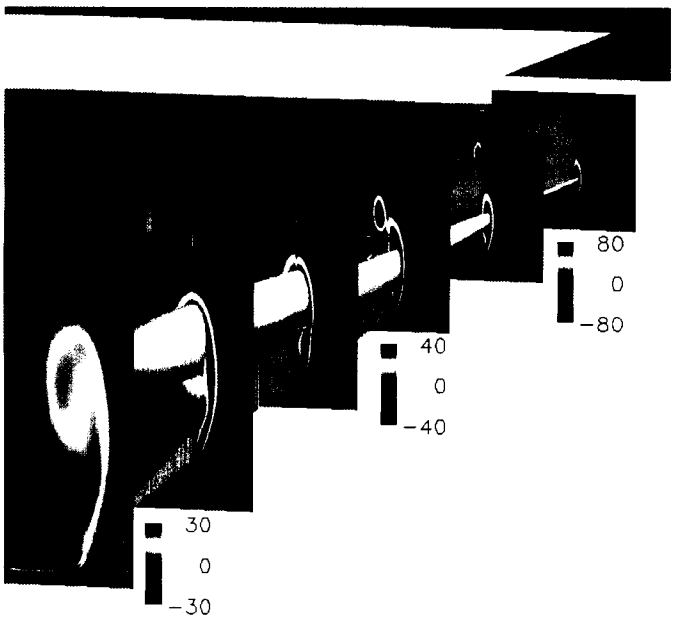

3(a) Untreated case.

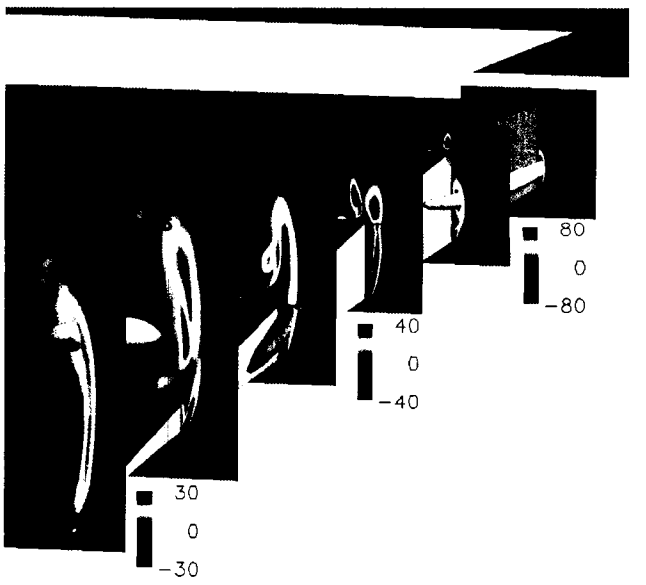

3(b) Treated case (configuration A16 from Table 1).

Figure 3. Global view of streamwise vorticity and isosurfaces of Cp (indicated by gray structures adjacent to the side edge).

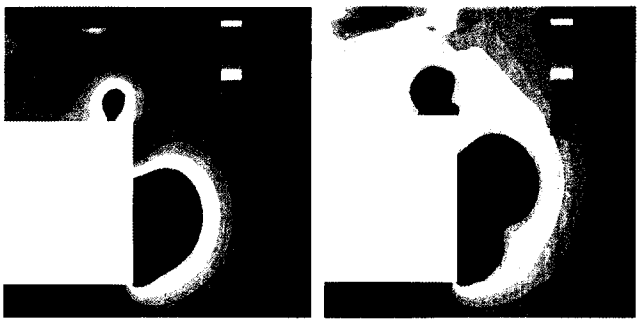

Figure 4. Cp contours at x=1.01 (In Figs. 4–7, the untreated case is shown on the left, and the treated case (configuration A16 from Table 1) is show on the right.)

Figure 5. Cp contours at x = 1.04.

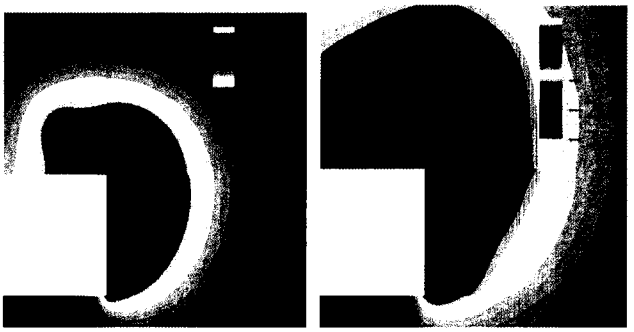

Figure 6. Cp contours at x = 1. 06.

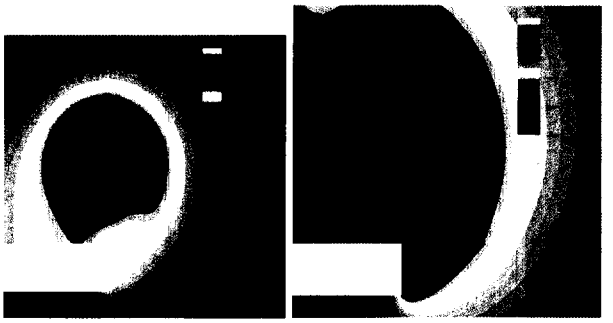

Figure 7. Cp contours at x = 1.11.

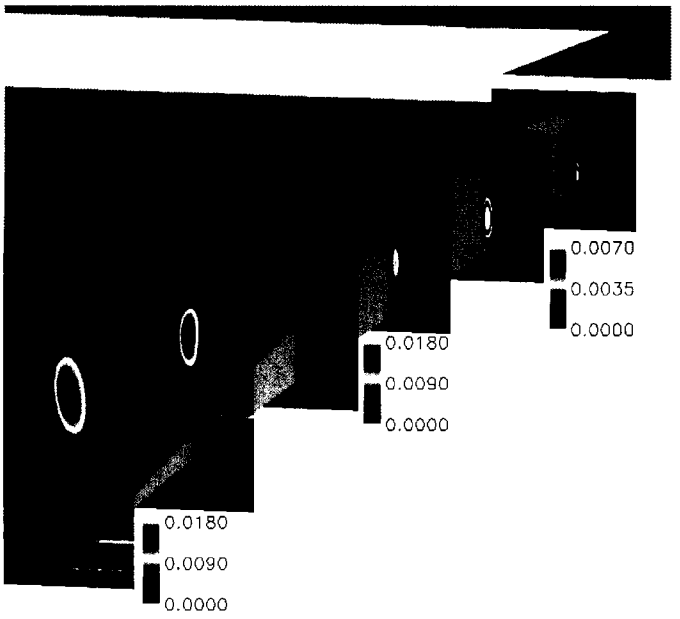

8(a) Untreated case.

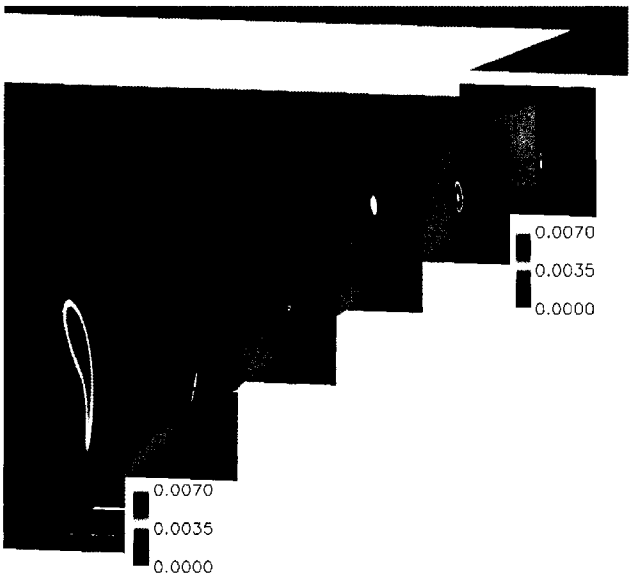

8(b) Treated case (configuration A16 from Table 1).

Figure 8. TKE distribution predicted by Menter's SST model.

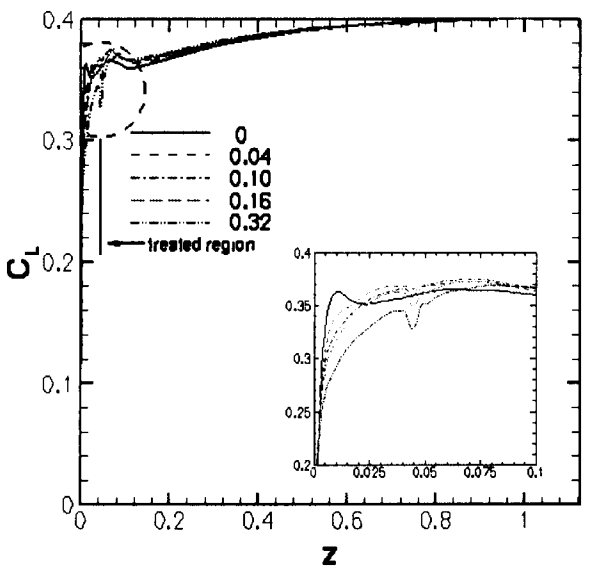

Figure 9. Variation of sectional lift based on pressure distribution over flap.

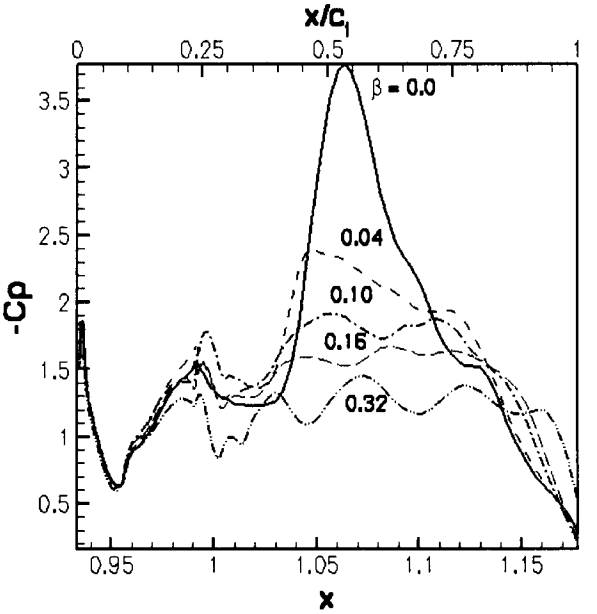

Figure 10. Cp distribution along top edge of flap tip surface: effect of flow admittance parameter.

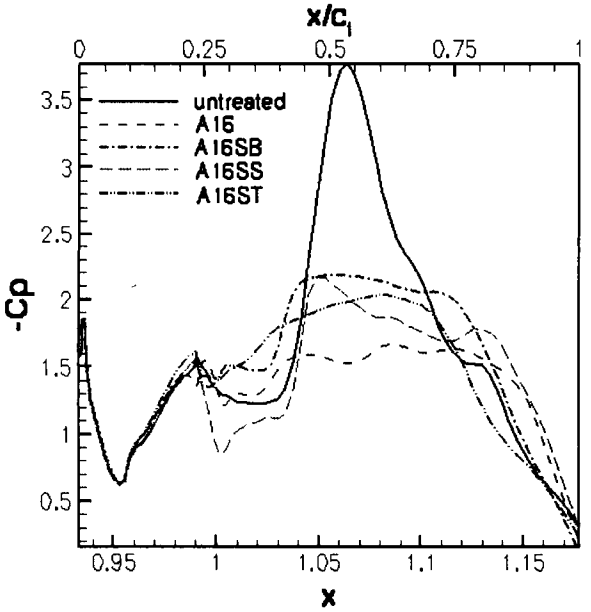

Figure 11. Cp distribution along top edge of flap tip surface: effect of sealing individual segments of the treated surface.

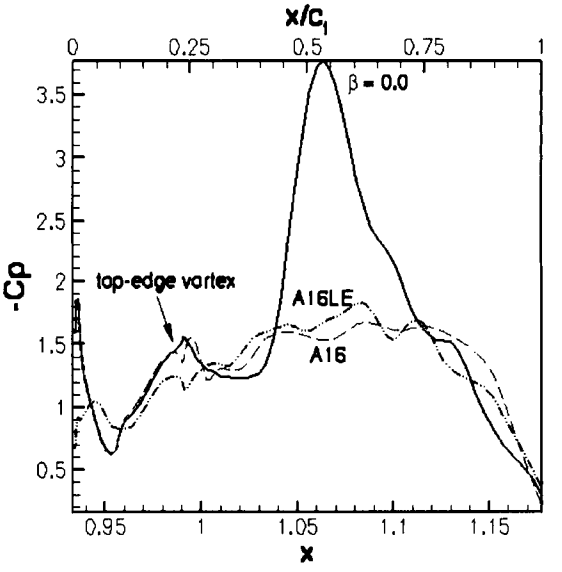

Figure 12. Cp distribution along top edge of flap tip surface: effect of extending treatment to leading edge.

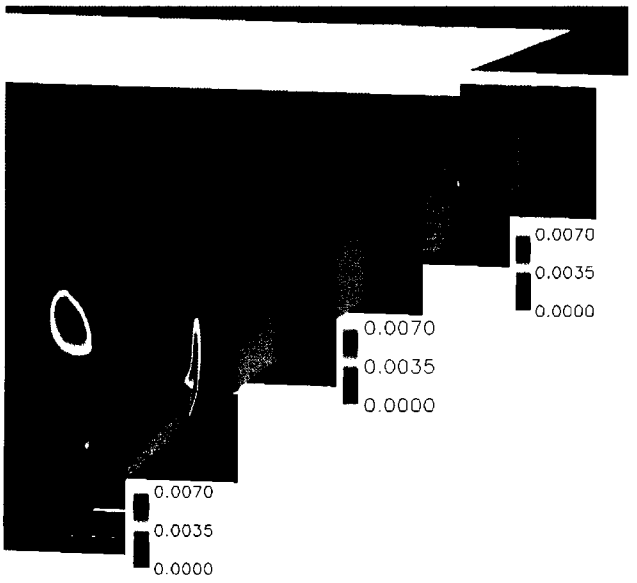

Figure 13. Effect of extending treatment to leading edge on TKE distribution.

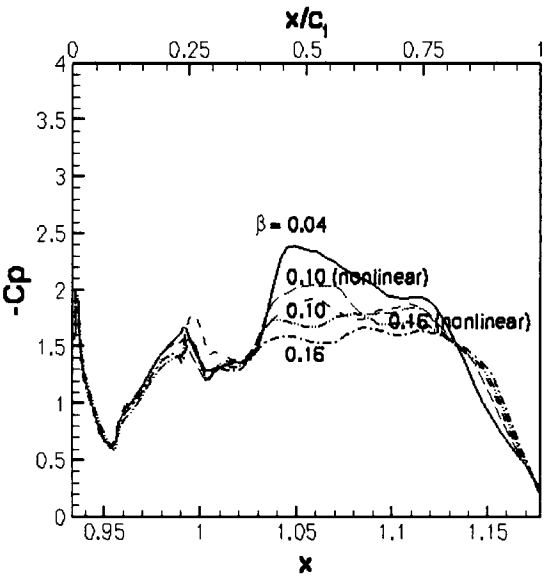

Figure 14. Cp distribution along top edge of flap-tip surface: effect of velocity-dependent pressure loss across porous skin.